Interplay between quantum diffusion and localization in the atom-optics kicked rotor

S. Sagar Maurya ⬤, J. Bharathi Kannan, Kushal Patel, Pranab Dutta, Korak Biswas ⬤,
Jay Mangaonkar ⬤,* M. S. Santhanam,† and Umakant D. Rapol ⬤‡
Department of Physics, Indian Institute of Science Education and Research, Pune 411008, India

Atom-optics kicked rotor represents an experimentally reliable version of the paradigmatic quantum kicked rotor system. In this system, a periodic sequence of kicks are imparted to the cold atomic cloud. After a short initial diffusive phase the cloud settles down to a stationary state due to the onset of dynamical localization. In this paper, to explore the interplay between localized and diffusive phases, we experimentally implement a modification to this system in which the sign of the kick sequence is flipped after every *M* kicks. This is achieved in our experiment by allowing free evolution for half the Talbot time after every *M* kicks. Depending on the value of *M*, this modified system displays a combination of enhanced diffusion followed by asymptotic localization. This is explained as resulting from two competing processes—localization induced by standard kicked rotor type kicks, and diffusion induced by the half Talbot time evolution. The experimental and numerical simulations agree with one another. The evolving states display localized but nonexponential wave function profiles. This provides another route to quantum control in the kicked rotor class of systems.

I. INTRODUCTION

The kicked rotor (KR) model has been extensively investigated as a paradigmatic model of both classical and quantum chaos [1,2]. The atom-optics based kicked rotor (AOKR) is an experimentally realizable analog of the KR model in which an ensemble of cold atoms are periodically kicked by sinusoidal potentials formed by a counterpropagating standing wave of light [3–6]. The classical limit of AOKR is chaotic for sufficiently strong kick strengths and exhibits intrinsic stochasticity in its dynamics. In this limit, KR behaves similar to a random walk. As the kicks impart energy to the system, diffusive growth of mean energy is observed. In contrast, the quantum regime entirely suppresses the classical diffusive growth beyond a short break time due to destructive quantum interferences [1]. This is the regime of dynamical localization and is the momentum-space analog of Anderson localization in real space. This shows up as wave functions localize in the momentum space $\psi_p \sim e^{-p/\xi}$, where p labels discrete momentum basis states and ξ is the localization length. Furthermore, AOKR and its variants are studied in other fields—condensed matter physics [7,8], molecular physics [9,10], and quantum information [11,12]—to explore quantum correlations to many-body localization. See Ref. [1] for a recent review of variants and applications of a kicked rotor system.

For many applications in the emerging areas of quantum technologies, it is important to be able to control the quantum effects. In the context of AOKR, the ability to control localization length and the energy of localized states can be useful [13]. Dynamical localization is generally destroyed by the addition of noise through decoherence processes and does not provide a means of quantum control. For example, it has been shown that decoherence in the form of noise [14–16], coupling with the rotor [17], and quantum measurements [11] can destroy dynamical localization. However, surprisingly, it was shown experimentally that Levy noise added to kick sequences of AOKR could control the decoherence rate and even the mean energy of localization, the Levy parameter in the noise distribution acting as the control parameter [18]. More conventional routes to exercise control is by manipulating the phases of the initial wave functions. For instance, it was shown previously that quantum-chaotic diffusion can be enhanced or suppressed by controlling the phases of the initial states [19,20]. However, in order to control the localization length, the unitary evolution operator that evolves the initial state needs to be changed and is not achievable by just controlling the phase of the initial state. In one such novel control scheme, introduced by Gong *et al.* [21], the phase of the kicking field is flipped periodically. By changing the sign of the kicking potential after *M* kicks (corresponds to introducing a phase shift among rotor momentum states), a significant change in the dynamical localization and quantum diffusion was observed. This variant of AOKR is different from the amplitude-modulated KR systems [22] in which the kick strength is varied. Quantum control in the context of AOKR has been experimentally realized by phase modulation [23,24] and in laser-kicked molecular rotors using time delay [13].

In the present paper, we experimentally realize a protocol of quantum control (similar in spirit to the one introduced in Ref. [21]) of diffusive and localized phases by appropriate

*Present address: Physikalisch-Technische Bundesanstalt (PTB),
Bundesallee 100, Braunschweig 38116, Germany.
†santh@iiserpune.ac.in
‡umakant.rapol@iiserpune.ac.in

modulation of the perturbations. Effectively, the sign of the kick strength in the KR system is periodically flipped. This is achieved using periodic time delayed kicks after a certain number of standard kicks that induce dynamical localization. Quite remarkably, this simple modification of kick sequences in AOKR does not destroy localization but leads to an enhancement of quantum energy at which localization takes place. In contrast to the earlier work [21] that depends on the presence of classical transporting islands in phase space for energy enhancements, we show that enhancements arise from a competition between two time periodic sequences in the AOKR system.

At this point, we emphasize the crucial differences between the standard KR and the AOKR. AOKR is a system of kicked atoms moving on a line, whereas the standard KR can be visualized as rotors moving on a circle. With a sufficiently broad initial distribution of momenta, the dynamics of AOKR involves the play of different quasimomenta β, whereas for the standard KR it is generally restricted to $\beta = 0$. Due to these differences, the modified kicked rotor (MKR) is presented as a motivation and a benchmark for the main ideas. All the experimental results are compared, not with MKR, but with the simulations of the Floquet operator of the AOKR averaged over quasimomenta β.

The MKR is introduced in Sec. II, and the modified *atom-optics* kicked rotor (MAKR) presented at the end of that section. The experimental and simulation results are reported in subsequent sections.

II. MODIFIED ATOM-OPTICS KICKED ROTOR

The system of interest is a modified form of kicked rotor given by [21]

$$ H = \frac{p^2}{2} + K \cos(x) \sum_n f_M(n)\delta(t - n), \tag{1} $$

where p and x denote the dimensionless momentum and position, respectively, K is the chaos parameter, and time t is scaled by the pulse period T such that $t \rightarrow t/T$. If $f_M(n) = 1$, then Eq. (1) is just the standard KR. In this paper, $|f_M(n)| = 1$, and $f_M(n)$ changes sign after every M kicks. In rest of this paper, Eq. (1) will be referred to as the MKR model, and it can be thought of as a specific realization of a generalized KR model in Ref. [25]. By discretizing the Hamilton's equation of motion corresponding to Eq. (1), a formal map connecting the position and momentum variables at time n and $n + 2M$ with $M \geqslant 1$ can be written down as

$$ x_{n+2M} = F_1(x_n, p_n), \quad p_{n+2M} = F_2(x_n, p_n). \tag{2} $$

In this, $F_1(,)$ and $F_2(,)$ are the map functions. In general, these map functions are sufficiently simple for the stardard kicked rotor but can be get increasingly cumbersome to write down explicitly for $M \geqslant 2$. However, numerical determination of the stroboscopic map is straightforward.

In Fig. 1 the classical stroboscopic section of KR (a), MKR with $M = 2$ (b), and with $M = 3$ (c) for kick strength $K = 5$ is shown. As evident in Fig. 1(a), the phase space is largely chaotic with a few regular islands. An ensemble of initial conditions launched from these islands will remain bound
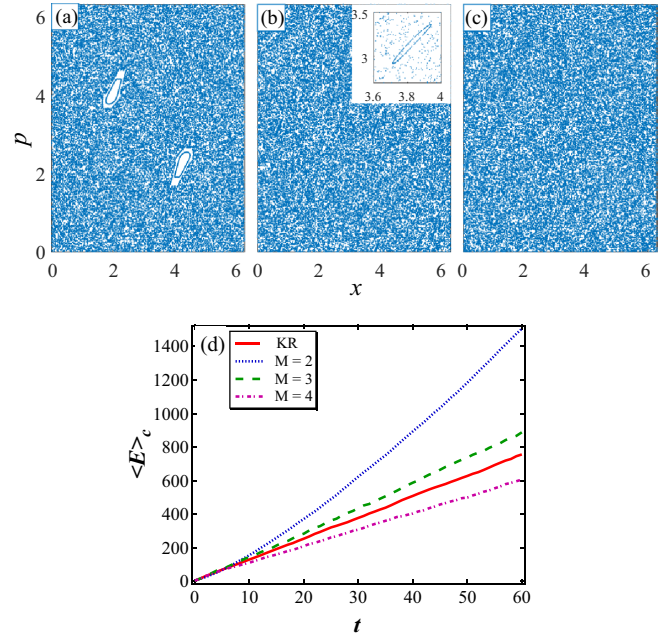

FIG. 1. Stroboscopic plots of the standard ($M = 0$) and modified kicked rotor ($M > 0$). The parameters are kick strength $K = 5$ and (a) $M = 0$, (b) $M = 2$, and (c) $M = 3$. The regular islands in the chaotic sea in (a) are nontransporting whereas those in (b) are transporting in nature, albeit much smaller in size. The inset in (b) shows an enlarged view of one of these islands. No regular structures are visible in (c). The classical energy $\langle E \rangle_c$ growth for various vales of M at $K = 5$ is shown in (d).

to these islands. In the case of MKR with $M = 2$, special nonchaotic structures called transporting trajectories exist in phase space as seen in the inset of Fig. 1(b). Transporting islands are present in many periodically driven dynamical systems, e.g., standard map [26], Hamiltonian ratchets [27], atomic KR [28,29], and are usually referred to as the accelerator modes because they support ballistic classical diffusion, i.e., $\langle E \rangle_n \propto n^2$, where n is the no of kicks. The quantum accelerator modes have been realized in cold atom experiments [30–32]. In the MKR, anomalous diffusion is observed in which $\langle E \rangle_n \propto n^\gamma$ with $1 < \gamma < 2$. Physically, this situation arises due to the "stickiness" of the boundary between the transporting trajectories and the chaotic sea. In contrast, the phase space is chaotic for $M = 3$ [Fig. 1(c)] and leads to normal diffusion. The classical energy $\langle E \rangle_c$ growth versus the number of kicks is shown in Fig. 1(d) for various M values. Due to the presence of transporting islands, it is clear that the classical energy growth is enhanced for $M = 2$ when compared that for other values of M. It also exhibits anomalous diffusion compared to other values of M, which shows linear diffusion. The transporting islands play a significant role in quantum dynamics even though their area in the phase space is tiny [21]. The presence of these transporting trajectories is ambiguous for MKR with larger values of M [21]. Now let us explore the quantum dynamics of MKR in the parameter space where transporting trajectories are present in their classical phase space of MKR with $M = 2$ as seen in Fig. 1(b) and compare it with the properties of KR. The quantum dynamics of MKR can be obtained by solving the time-dependent
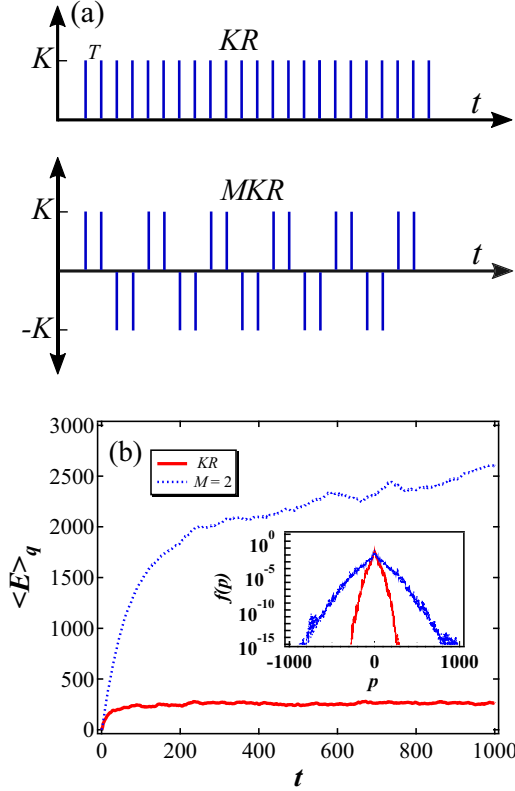
FIG. 2. (a) Pulse scheme for the regular and modified kicked rotor at $k = 5$ and $\hbar_{\mathrm{eff}} = 1$ ($K = 5$). For $M = 2$, the sign of K is flipped alternatively. (b) Simulated energy evolution of KR (dashed line) and MKR with $M = 2$ (solid line). The quantum energy $\langle E \rangle_q$ for $M = 2$ localizes at a higher energy. Inset plots (on a semilogarithmic scale) the momentum distribution of for the same at $t = 1000$.

Schrödinger equation corresponding to the MKR Hamiltonian. The split evolution technique is implemented to evolve the initial state according to the Schrödinger equation [26].

To build the quantum dynamics of MKR, let us consider the period-1 Floquet operator corresponding to the standard kicked rotor $\widehat{F}_{\mathrm{KR}}^{\pm}$ for which $f_M(n)$ is a constant, i.e., $f_M(n)$ is either $+1$ or -1 for all n's.

Thus, the required operator is

$$\widehat{F}_{\mathrm{KR}}^{\pm} = \exp\left[i\frac{\hbar_{\mathrm{eff}}}{2}\frac{\partial^2}{\partial x^2}\right]\exp\left[\mp i\frac{K}{\hbar_{\mathrm{eff}}}\cos(x)\right], \quad (3)$$

where $\hbar_{\mathrm{eff}} = T\hbar$ is the scaled Planck's constant, $k = K/\hbar_{\mathrm{eff}}$ denotes the strength of phase modulation imparted by the kicks. Using this as the building block, the Floquet operator for MKR can be constructed as M application of $\widehat{F}_{\mathrm{KR}}^{+}$ followed by M application of $\widehat{F}_{\mathrm{KR}}^{+}$. Thus, for MKR, we obtain

$$\widehat{F}_{\mathrm{MKR}} = (\widehat{F}_{\mathrm{KR}}^{-})^M (\widehat{F}_{\mathrm{KR}}^{+})^M. \quad (4)$$

To implement this Floquet Hamiltonian in an atom-optics experiment, the sign of the phase modulation must change with periodicity M as dictated by Eq. (4). The kicking scheme of Eq. (4) is shown in Fig. 2(a) and simulated time evolution of mean quantum energy $\langle E \rangle_q$ is shown in Fig. 2(b) for KR and MKR with $M = 2$. The inset in Fig. 2(b) represents momentum distribution. However, this type of Hamiltonian is

difficult to realize in experiments since it involves an abrupt sign change of the kicking potential after M kicks. An alternative method to realize MKR is by introducing controlled time delays after every M kicks [21]. Consider a wave function of the system $\Psi(x, t)$ at any time t. This can be expanded in the momentum basis as

$$\Psi(x, t) = \sum_m A_m \langle x | m \rangle, \quad (5)$$

with A_m being the expansion coefficients. The flipping of the sign of K can also be thought of as a shift in the spatial coordinate by π since $K\cos(x + \pi) = -K\cos x$. Hence, it is convenient to use $x \to x + \pi$ instead of $K \to -K$. Now, to see its effect on the momentum basis states, let us consider

$$\begin{aligned}\Psi(x + \pi, t) &= \sum_m A_m \langle x + \pi | m \rangle \\ &= \sum_m A_m \exp i(x + \pi)m \\ &= \sum_m (-1)^m A_m \langle x | m \rangle.\end{aligned} \quad (6)$$

It is clear that the change in sign of kicking strength effectively introduces a phase difference of π between the neighboring states. This phase difference can also be generated by introducing time delays in the system. To see this, consider the action of a free-evolution operator of MKR for $t = T$ acting on a momentum state,

$$\exp(ip^2 T/2\hbar)|m\rangle = \exp(im^2\hbar T/2)|m\rangle. \quad (7)$$

From this, we can estimate the duration of free evolution T_d required to obtain a phase difference of π between neighboring momentum states. For a phase difference of π, the condition to be satisfied is $\exp\{i\hbar T_d[(m+1)^2 - m^2]/2\} = \exp(i\pi)$, and from this we get the time duration to be

$$T_d = \frac{2\pi}{\hbar} = \frac{2\pi T}{\hbar_{\mathrm{eff}}}. \quad (8)$$

This delay corresponds to half the Talbot time and has the same effect as flipping the sign of the kick strength between the pulses [21]. Figure 3(a) shows the kicking scheme for MAKR with $M = 2$, 3 and 4. including the delay time T_d. Due to the presence of two periods, the system is no longer periodic with time period T but has an effective period of $T(M - 1) + T_d$. Thus, the Floquet operator for the modified *atom-optics* kicked rotor $\widehat{F}_{\mathrm{MAKR}}$ is given by

$$\begin{aligned}\widehat{F}_{\mathrm{MAKR}} &= \left(\exp\left[-i\frac{\hbar T_d}{2}(\hat{p} + \beta)^2\right]\exp\left[-i\frac{K}{\hbar_{\mathrm{eff}}}\cos(\hat{x})\right]\right) \\ &\quad \times \left(\exp\left[-i\frac{\hbar_{\mathrm{eff}}}{2}(\hat{p} + \beta)^2\right]\exp\left[-i\frac{K}{\hbar_{\mathrm{eff}}}\cos(\hat{x})\right]\right)^{M-1} \\ &= \widehat{\mathbf{F}}_{\mathrm{KR}}\widehat{F}_{\mathrm{KR}}^{M-1}.\end{aligned} \quad (9)$$

where $\hat{p} = -i\frac{\partial}{\partial x}$ and β is the quasimomentum. In this, $\widehat{F}_{\mathrm{KR}}^{M-1}$ denotes $M - 1$ applications of $\widehat{F}_{\mathrm{KR}}$ for time duration T, and $\widehat{\mathbf{F}}_{\mathrm{KR}}$ denotes the application of the kicked rotor Floquet operator with a free propagation time of T_d. The existence of two time periods T and T_d in the atom-optics version of the kicked rotor system makes it different from the standard KR system.
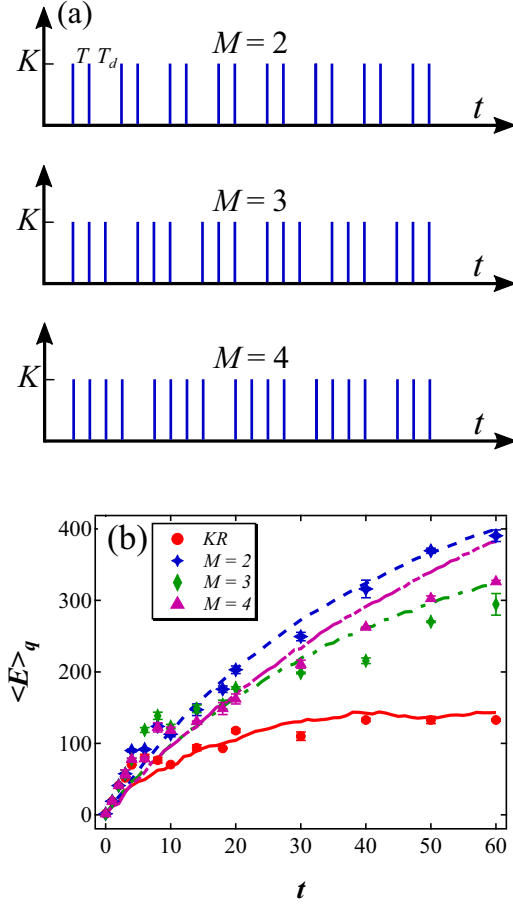
FIG. 3. (a) Kicking scheme for MAKR with $M = 2-4$. This scheme also shows the delay time T_d. (b) Mean quantum energy $\langle E \rangle_q$ evolution for different values of M at $k = 5$ and $\hbar_{\mathrm{eff}} = 1$. The solid lines and markers indicate the numerical simulation and the experimental data, respectively.

It is worth pointing out that when studying resonance phenomena for a finite-temperature cloud, we should take into account $\beta \neq 0$ since all the quasimomentum subspaces are initially populated. The Floquet operator governing the dynamics in each quasimomentum subspace is explicitly dependent on β [see Eq. (9)]. This leads to the overall dynamics exhibiting significant differences when compared to the case of standard QKR in which case the dynamics are restricted to the $\beta = 0$ subspace. At antiresonance AOKR exhibits a significant momentum spread and a diffusive growth of the particle energy, whereas the energy of the standard QKR is localized [33]. In a thermal cold atom cloud, atoms have a non-negligible initial velocity relative to the standing wave potential, and this noninteger quasimomentum determines the behavior under half-Talbot time kicking. Before the results are discussed, a brief review of the experimental procedure is in order.

III. ATOM-OPTICS EXPERIMENTAL SETUP

First, we discuss the experimental setup. The variables and parameters of the kicked rotor system and AOKR are related as follows: $x \rightarrow 2k_L x$, $p \rightarrow 2k_L T\, p/m$, and $\hbar_{\mathrm{eff}} = 8\omega_r T$

where k_L, m, and ω_r are the wave numbers of the optical lattice beam, mass of the atoms and recoil frequency, respectively. The amplitude modulation depth or the kick strength is $k = \hbar\Omega^2\tau/8\Delta$, where Ω, Δ, and τ are the resonant Rabi frequency, the detuning of the light used to create the optical lattice potential, and the pulse duration, respectively. The experimental setup is the same as described in Ref. [18]. We create a cold thermal ensemble of ^{87}Rb consisting of 2×10^5 atoms every 12 s in a crossed optical dipole trap. The temperature of the thermal cloud is about 5 μK. Before the optical standing wave pulses are applied, the atoms are present in the $|F = 1, m_F = -1\rangle$ state. The laser used for realizing the standing wave is locked to the $|5\,S_{1/2}, F = 2\rangle \rightarrow |5\,S_{3/2}, F' = 2\rangle$ D2 transition at 780 nm and is, thus, 6.8 GHz red-detuned from the atom's accessible transition. To synthesize the MKR Hamiltonian, the off time between the δ pulses is adjusted. The on-time τ of the standing wave is kept as 100 ns.

The experimental setup and the implementation sequence is the same as reported in Ref. [18]. The quantum AOKR is governed by two dimensionless parameters: $\hbar_{\mathrm{eff}}$ and K. To keep K fixed, k is adjusted for different values of $\hbar_{\mathrm{eff}}$. To calibrate the kick strength k, we use Raman-Nath diffraction on an almost ideal zero-momentum state, i.e., a Bose-Einstein condensate. The number of atoms in the nth momentum state after undergoing diffraction is a Bessel function $J_n^2(k)$. Thus, k can be accurately determined by measuring the distribution and fitting it to this Bessel distribution [34]. As mentioned before, for MKR, we use a time delay of half-Talbot time ($\sim$33.17 μs for ^{87}Rb and $2\pi/k_L = 780$ nm) to introduce appropriate phase relations between the diffracted wave packets. The timing error fluctuations are on the order of picoseconds ensuring good control over tuning this phase according to the Hamiltonian. The optical lattice is arranged in a retroreflected configuration, making it more stable against vibrational phase noise.

IV. EVOLUTION OF MEAN ENERGY

In experiments, the initial state consists of an ensemble of atoms with a finite momentum spread. In order to model a thermal cloud of cold atoms, numerical simulations are performed using Eq. (9) operating on a Gaussian distributed momentum state,

$$|\psi(t = 0)\rangle = \int_{-1/2}^{1/2} d\beta \sum_{p=-\infty}^{\infty} D_p(\beta)^{1/2}|p + \beta\rangle, \quad (10)$$

where $p \in \mathbb{Z}$, and $D_p(\beta) = \frac{1}{w\sqrt{2\pi}} \exp(-\frac{(p+\beta)^2}{2w^2})$ is the Gaussian momentum distribution with zero mean and standard deviation w as a function of quasimomenta $\beta \in (-1/2, 1/2)$ [33]. In practice, the summation over p in this equation is carried out over only a finite set of momentum basis states.

A. $M = 2$ case

The kicking scheme for MKR is shown in Fig. 3(a). The time evolution of mean quantum energy from the numerical simulations of MKR using Eq. (4) is shown in Fig. 3(b).

For the standard KR, the mean energy displays the expected linear increase for short times (within break-time t_b of order $K^2/2$). For $t > t_b$, the quantum effects become significant, and dynamical localization is realized. For the same set of parameters as that for KR except that $M = 2$ a pronounced enhancement in the saturated energy is evident in this figure. Dynamical localization occurs for $M = 2$ as well. In the case of MKR with $M = 2$ and $K = 5$, transporting trajectories are present in phase space as seen in Fig. 1(b). Thus, as argued in Ref. [21] in the quantum regime, the mean energy corresponding to MKR is enhanced with respect to the standard KR. Furthermore, the width of momentum distribution [shown as the inset in Fig. 2(b)] is also significantly enhanced for MKR compared with KR. For other parameters as well, transporting islands lead to an enhancement in quantum energy upon depending on the size of the island [21]. In this paper, due to experimental constraints, we will work with the parameters used in Fig. 2 along with $M = 3, 4$.

Now, we will compare this phenomenology with the experimental results. Figure 3(a) shows the kicking scheme for MAKR with $M = 2$–4 including the delay times T_d. Figure 3(b) displays the corresponding results for mean energy evolution from our atom-optics experiment. This figure shows both the experimental data (solid symbols) as well as the numerical simulations (lines) of MAKR obtained using the Floquet operator in Eq. (9). A good agreement is observed between the experimental and numerical simulations. At first sight, it is tempting to attribute the energy enhancement seen in the experiment entirely to the presence of transporting islands. However, these islands exist in phase space only over a small range of K. In the experiment, the value of kick strength K suffers from approximately 10% error that washes out most of the contribution arising from transporting islands. Furthermore, the quantum contribution depends on the value of effective Planck's constant $\hbar_{\text{eff}}$ relative to the classical phase space structure whose effect is being probed [35]. In our case, the values chosen for $\hbar_{\text{eff}}$ are large relative to the small area of transporting islands. Hence, the quantum contribution of these island structures is not very significant. Bulk of the enhancement arises due to the presence of two timescales T and T_d in the MAKR system. An interesting interplay between the two time periods T and T_d is seen. The time evolution with a pulse period of T along with the kick strength k is arranged such that it induces localization in the system. For an initial state with significant momentum spread ($w \gtrsim 1$) a pulse period corresponding to half-Talbot time T_d leads to a linear diffusive growth in energy [6,33]. The dynamics of MAKR is governed by the competition between these contrasting behaviors of localization and diffusion.

In our experiments, the MAKR system can be evolved only up to 60 kicks due to constraints of the experimental arrangement. For a finite number of total kicks N applied to the atomic cloud, the number of the (diffusion inducing) free-evolution phase with time period T_d is $N_d = N/M$. The number N_l of the localization-inducing evolution phase with time period T is $N_l = (M-1)N_d$. Thus, if $M \gg 1$, then $N_l \gg N_d$. In this scenario, localization effects dominate, and diffusion is suppressed. This corresponds to the standard KR limit [the lowermost curve (red curve) in Fig. 3(b)]. In the other limit, as $M \to 1$, diffusive growth of energy is strongly

favored over localization. The competition between these processes determines the enhancement of saturated energy in the MAKR system. In a short timescale, the localization is destroyed by antiresonance, but eventually localization sets into the system due to destructive interference in the momentum space. In particular, the contribution of classical transporting islands is not very significant. For $M = 1$, diffusion is dominant, and localization is completely suppressed. For $M = 2$, we get $N_d = N_l$. Hence, we can anticipate localization as well as the diffusive phase. Consistent with this constraint, both the experiment and the numerics [blue color in Fig. 3(b)] show an enhancement induced by the diffusive phase as well as localization in the form of saturated mean energy.

In particular, we emphasize that the contribution of classical transporting islands is not very significant for $M = 2$. This argument presented above also implies that the enhancement in saturated energy should be seen for $M = 3, 4$ as well even though classically no transporting islands are present in phase space [see Fig. 1(c)]. We will consider these cases in the next section.

B. Case of $M > 2$

For $M > 2$, $N_l > N_d$. This guarantees that localization can be seen for all $M > 2$'s. However, since N_d decays as M increases, the diffusive phase weakens. Hence, at any given number of kicks, the highest energy reached for $M > 2$ will always be less than that for $M = 2$. Figure 3(b) displays quantum energy $\langle E \rangle_q$ against the number of kicks for $K = 5$ and $\hbar_{\text{eff}} = 1$ for MAKR for $M = 3$ and $M = 4$. Even for $M = 3, 4$, a significant enhancement in the energy is seen. This is purely attributed to the half-Talbot time evolution's T_d in the kicking sequence as the classical phase space is completely chaotic. As argued in the previous section, two competing effects are at play—localization induced by the evolution over time-period T and diffusion due to time delay T_d. The long-time behavior of MKR would exhibit complete localization [21], even though it is not apparent in Fig. 3(b) due to the small number of kicks in the experiment.

From Fig. 4(a) of the momentum distribution in the semilogarithmic scale for KR and MAKR with $M = 2$–4 deduced from absorption images shown in Fig. 4(b). It is clear that the width of the distribution is larger for $M = 2$–4 as compared to that of standard KR. This is also visible in the absorption images that carry more weight in the higher momentum states. After many kicks, numerical simulations begin to deviate from experimental data in Fig. 4 due to errors in deducing the number of atoms in the higher momentum states via absorption imaging. The experimental momentum distribution for $M = 2$–4 are qualitatively similar and show a nonexponential profile. Hence, the localization length is not a good measure to quantify the extent of localization.

For a wave function (in momentum representation) $\langle m|\psi \rangle$, one of the commonly used localization measures is the inverse participation ratio (IPR), defined as [36]

$$I_D = \sum_{m=1}^{D} |\langle m|\psi \rangle|^4, \tag{11}$$
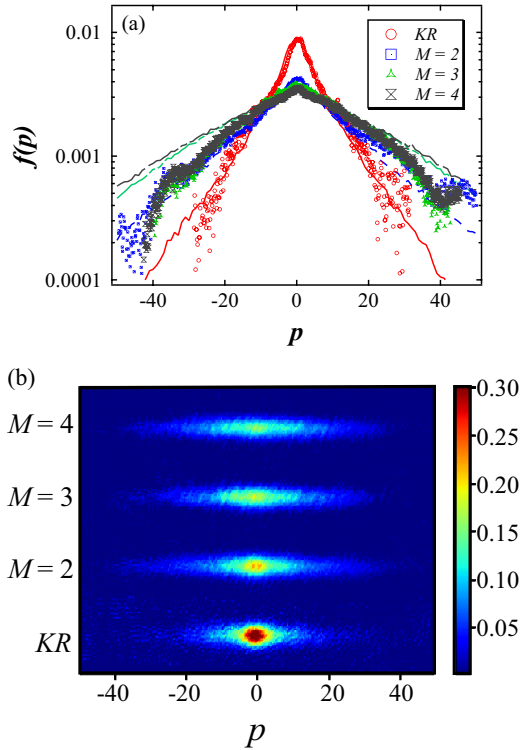
FIG. 4. (a) Momentum distribution profiles for $M = 0, 2, 3$ and 4 at the parameters $K = 5$ and $\hbar_{\rm eff} = 1$. The markers and solid lines denote experimental and simulated momentum profiles, respectively. $M = 2$ clearly shows enhanced localization length. (b) Absorption images for different values of M with $\hbar_{\rm eff} = 1$ and $K = 5$.

where D is the dimension of the Hilbert space in which $\langle m|\psi \rangle$ resides. A localized wave function will have $I_D \sim 1$, whereas for a completely delocalized wave function $I_D \propto 1/D$. Smaller values of I_D correspond to wave functions spread over larger set of basis states. As evident in Fig. 5, the IPR for $M = 2$–4 all have a much lower value compared to the KR, implying the spread in the momentum distribution and energy enhancement compared to KR. But I_D for $M = 2$–4 are very close to each
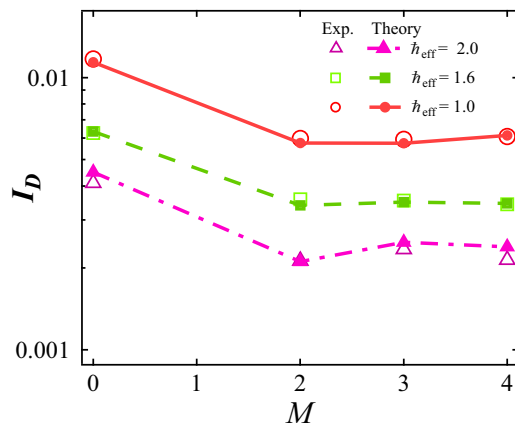

FIG. 5. IPR for experimental data as a function of M for different values of $\hbar_{\rm eff}$ whereas maintaining the kick strength constant at $K = 5$. Errors bars for experimental data lie within the marker, hence, they are not shown here.

other, indicating that the spread is almost the same for all of them. As transporting islands of significant size are only present in the case of MKR with $M = 2$ ($k = 5$), one would expect to have a maximum energy enhancement and momentum distribution spread for $M = 2$ [21]. But in our case, we observe the momentum distribution to be very close to each other for all the $M = 2$–4. This implies that the enhancement in the localization length or momentum distribution spread arising from transporting islands for $M = 2$ is less significant in MAKR. The dynamics is largely determined through the interplay of two time periods in the system. It has been shown that very small changes to the system parameters (k and $\hbar_{\rm eff}$) can lead to the destruction of transporting islands present in the classical phase space and nonexponential shape of quantum momentum distribution [21]. This change in the line shape for dynamical localization even occurs without causing an obvious difference in energy absorption behavior. A similar type of enhancement of dynamical localization length and energy absorption is observed for various values of M and for a range of parameters k and $\hbar_{\rm eff}$ in the MKR model. The only requirement being that k should be sufficiently large for dynamical localization to take place in the system. As in the standard KR, the experimental data in Fig. 5 shows that for a fixed M, a decrease in $\hbar_{\rm eff}$ is associated with broadening of the wave function profile. Hence, I_D increases as $\hbar_{\rm eff} \to 0$.

V. CONCLUSIONS

In this paper, we have studied a modified kicked rotor model as well as its experimental implementation in an equivalent atom-optics based test bed. The model considered here is the modified atom-optics kicked rotor model in which the sign of the kick strength (in the standard KR) is flipped after every M kicks. In the experiment, the modified atomic kicked rotor is realized by introducing appropriate time delays (equal to half-Talbot time) in the kicking sequence, which is equivalent to flipping the sign of the kick strength. Introduction of periodic time delays in the KR system creates drastic changes in the dynamics as a result of two competing effects—one is the localization effects induced by periodic kick sequences of time period T and the other is the diffusive effects induced by sequences with delay time T_d equal to the half-Talbot time. It is shown that the modified atom-optics kicked rotor system with $M = 2$–4 shows enhanced quantum mean energies when compared to the standard kicked rotor model. The competition between the two time periods, T and T_d, explains the observed mean energy dynamics and it is not dependent on the presence or absence of the transporting islands in classical phase space. Whereas quantum mean energy enhancement can be engineered by taking advantage of the presence of transporting islands in classical phase space, it provides a somewhat restrictive framework. In contrast, this paper emphasizes that quantum mean energy enhancement is possible without replying on classical features in the atom-optics kicked rotor. This is shown through numerical simulations of AOKR and in the experiments.

These results are of intrinsic interest in the quantum chaos of kicked rotor, but also in the broader context of quantum control. Techniques to control the quantum systems with

classically chaotic behavior has become an active area of research interest over the years. Through this paper, we have demonstrated a control over the best-known phenomenon experimentally in quantum chaos. The dynamical localization can be enhanced over a wide range of parameters provided the system is classically chaotic. Apart from the atom-optics realization of KR and MKR, it would also be interesting to explore the dynamics of a molecular version of KR and MKR, i.e., diatomic cloud periodically kicked by strong microwave fields. Another promising direction to look at is the experimental realization of KR and MKR in a square-well potential [37]. Along this direction, an interesting model (which is very different from the one discussed here) has been proposed for the study of classical and quantum anomalous diffusion [38].

These efforts might lead to a broader understanding of diffusion and localization in time-dependent chaotic quantum systems.

ACKNOWLEDGMENTS

[1] M. S. Santhanam, S. Paul, and J. Bharathi Kannan, Phys. Rep. **956**, 1 (2022).

[2] G. Casati and B. Chirikov, *Quantum Chaos: Between Order and Disorder* (Cambridge University Press, New York, 1995).

[3] F. L. Moore, J. C. Robinson, C. F. Bharucha, B. Sundaram, and M. G. Raizen, Phys. Rev. Lett. **75**, 4598 (1995).

[4] H. Ammann, R. Gray, I. Shvarchuck, and N. Christensen, Phys. Rev. Lett. **80**, 4111 (1998).

[5] J. Ringot, P. Szriftgiser, J. C. Garreau, and D. Delande, Phys. Rev. Lett. **85**, 2741 (2000).

[6] M. B. d'Arcy, R. M. Godun, M. K. Oberthaler, D. Cassettari, and G. S. Summy, Phys. Rev. Lett. **87**, 074102 (2001).

[7] S. Fishman, D. R. Grempel, and R. E. Prange, Phys. Rev. Lett. **49**, 509 (1982).

[8] G. Benenti, G. Casati, I. Guarneri, and M. Terraneo, Phys. Rev. Lett. **87**, 014101 (2001).

[9] R. Blümel, S. Fishman, and U. Smilansky, J. Chem. Phys. **84**, 2604 (1986).

[10] I. S. Averbukh and R. Arvieu, Phys. Rev. Lett. **87**, 163601 (2001).

[11] P. Facchi, S. Pascazio, and A. Scardicchio, Phys. Rev. Lett. **83**, 61 (1999).

[12] B. Georgeot and D. L. Shepelyansky, Phys. Rev. Lett. **86**, 2890 (2001).

[13] M. Bitter and V. Milner, Phys. Rev. Lett. **118**, 034101 (2017).

[14] E. Ott, T. M. Antonsen, and J. D. Hanson, Phys. Rev. Lett. **53**, 2187 (1984).

[15] D. Cohen, Phys. Rev. A **44**, 2292 (1991).

[16] R. Graham and S. Miyazaki, Phys. Rev. A **53**, 2683 (1996).

[17] S. Paul and A. Bäcker, Phys. Rev. E **102**, 050102(R) (2020).

[18] S. Sarkar, S. Paul, C. Vishwakarma, S. Kumar, G. Verma, M. Sainath, U. D. Rapol, and M. S. Santhanam, Phys. Rev. Lett. **118**, 174101 (2017).

[19] J. Gong and P. Brumer, J. Chem. Phys. **115**, 3590 (2001).

[20] J. Gong and P. Brumer, Phys. Rev. Lett. **86**, 1741 (2001).

[21] J. Gong, H. J. Wörner, and P. Brumer, Phys. Rev. E **68**, 056202 (2003).

[22] D. Shepelyansky, Physica D **8**, 208 (1983).

[23] C. Hainaut, A. Rançon, J.-F. Clément, J. C. Garreau, P. Szriftgiser, R. Chicireanu, and D. Delande, Phys. Rev. A **97**, 061601(R) (2018).

[24] D. H. White, S. K. Ruddell, and M. D. Hoogerland, New J. Phys. **16**, 113039 (2014).

[25] I. Dana, E. Eisenberg, and N. Shnerb, Phys. Rev. E **54**, 5948 (1996).

[26] F. M. Izrailev, Phys. Rep. **196**, 299 (1990).

[27] H. Schanz, M.-F. Otto, R. Ketzmerick, and T. Dittrich, Phys. Rev. Lett. **87**, 070601 (2001).

[28] D. A. Steck, W. H. Oskay, and M. G. Raizen, Science **293**, 274 (2001) .

[29] W. K. Hensinger, H. Häffner, A. Browaeys, N. R. Heckenberg, K. Helmerson, C. McKenzie, G. J. Milburn, W. D. Phillips, S. L. Rolston, H. Rubinsztein-Dunlop and B. Upcroft, Nature (London) **412**, 52 (2001).

[30] M. K. Oberthaler, R. M. Godun, M. B. d'Arcy, G. S. Summy, and K. Burnett, Phys. Rev. Lett. **83**, 4447 (1999).

[31] R. M. Godun, M. B. d'Arcy, M. K. Oberthaler, G. S. Summy, and K. Burnett, Phys. Rev. A **62**, 013411 (2000).

[32] S. Fishman, I. Guarneri, and L. Rebuzzini, Phys. Rev. Lett. **89**, 084101 (2002).

[33] M. Saunders, P. L. Halkyard, K. J. Challis, and S. A. Gardiner, Phys. Rev. A **76**, 043415 (2007).

[34] J. Mangaonkar, C. Vishwakarma, S. S. Maurya, S. Sarkar, J. L. MacLennan, P. Dutta, and U. D. Rapol, J. Phys. B: At., Mol. Opt. Phys. **53**, 235502 (2020).

[35] M. Sheinman, S. Fishman, I. Guarneri, and L. Rebuzzini, Phys. Rev. A **73**, 052110 (2006).

[36] J. T. Edwards and D. J. Thouless, J. Phys. C **5**, 807 (1972).

[37] R. Sankaranarayanan, A. Lakshminarayan, and V. B. Sheorey, Phys. Rev. E **64**, 046210 (2001).

[38] R. Sankaranarayanan and V. B. Sheorey, Phys. Lett. A **338**, 288 (2005).